Available online at www.sciencedirect.com

SciVerse ScienceDirect

Physics Procedia 41 (2013) 302 – 311

Physics Procedia

Lasers in Manufacturing Conference 2013

Effects of the alloy composition on phase constitution and properties of laser deposited Ni-Cr-B-Si coatings

I. Hemmati*, V. Ocelík, J. Th. M. De Hosson

Materials innovation institute (M2i), Department of Applied Physics, University of Groningen, Nijenborgh 4, 9474 AG, Groningen, The Netherlands

Abstract

Three Ni-Cr-B-Si hardfacing alloy powders with different Cr contents and Si to B ratios were deposited at cladding speeds of 5-40 mm/s on steel substrate using laser beam and the alloy composition-phase formation-properties relationships in the deposits were studied using several experimental techniques. Two general groups of compositions could be defined in this alloy system; the high-alloy grades characterized by numerous Cr boride precipitates, a low Si/B ratio and substantial Ni-B-Si eutectics, and the low-alloy grades with very little Cr boride precipitates, a high Si/B ratio and limited amounts of interdendritic eutectics. The findings confirmed that phase formation of Ni-Cr-B-Si laser deposited coatings primarily depends on the Cr content and Si/B ratio with the former controlling the amount of Cr-rich precipitates and the latter influencing the nature of the eutectic structures. In addition, it is shown that both Cr-rich precipitates and eutectic structures contribute to the functional properties of the coatings such as hardness and cracking susceptibility. The correlation between phase constitutions produced by different compositions and the hardness/cracking tendency is established and discussed.

Keywords: Laser cladding, Ni hardfacing alloys, microstructure, alloy composition

* Corresponding author. Tel.:+31503634890; fax: +31503634881.
E-mail address: i.hemmati@rug.nl.

doi:10.1016/j.phpro.2013.03.082

1. Introduction

Ni-Cr-B-Si alloys are among the most widely used hardfacing alloys for wear and corrosion protection (Das et al., 2005; Planche et al., 2005). Although these alloys have been traditionally deposited by thermal spray and fuse techniques, laser cladding is being increasingly used to produce dense Ni-Cr-B-Si coatings with metallurgical bonding to the substrate and superior functional properties (Miguel et al., 2003; E. Fernández et al., 2005; Conde et al., 2002). Moreover, in recent years some Ni-Cr-B-Si alloys such as Colmonoy 6 (Paul et al., 2006) or Colmonoy 227-F (Angelastro et al., 2009) have also been used for free-form fabrication of functional components. Despite the growing application of these alloys in laser deposition and the multitude of commercial Ni-Cr-B-Si alloys (e.g. the Colmonoy family), there is not much data available in the literature about the correlation between alloy composition and phase formation, microstructure and properties of the laser clad Ni-Cr-B-Si deposits.

The previous study of the authors on laser deposited Ni-Cr-B-Si alloys with high contents of Cr and B showed that these alloys have a tendency to develop multiple microstructures from the same chemistry under different cooling rates, e.g. different cladding speeds or substrate temperatures (Hemmati et al., 2011). As the key alloying elements of this system are Cr, B and Si, three alloy powders with different contents of these elements were deposited using laser beam at different cladding speeds and the phase formation, microstructural evolution, hardness and cracking tendency of the rapidly solidified coatings were evaluated. Hence, the focus of this study will be on how variations of the key alloying elements of this system (i.e. Cr, Si, and B) affect the microstructure and properties of the coatings deposited at different cladding speeds. The findings of this work can enhance our understanding of the composition-phases-properties relationship in this important group of hardfacing alloys with the goal of developing alloy grades more suitable for laser deposition processes.

2. Experimental procedure

Laser cladding with powder injection was used to produce single-track and five-track deposits (33% track overlapping, 10 mm wide) with a thickness of 0.9-1.1 mm at cladding speeds of 5, 10, 20 and 40 mm/s. Three types of Ni-Cr-B-Si alloy powders with different contents of alloying elements were deposited on 50-mm-diameter S355 carbon steel rods using a continuous wave IPG fiber laser with a wavelength of 1.07 μm and laser powers of 800-1000 W. Chemical compositions of the coating and substrate materials are presented in Table 1. Powder feeding system consisted of Metco Twin 10C powder feeder, argon as carrier and shielding gas and a side cladding nozzle. To prevent cracking of the Colmonoy 69 clad layers, the substrate bars used for deposition of this alloy were preheated to 500 ^{o}C immediately before cladding using a tube furnace and the coated bars were left in the furnace to cool slowly down to the room temperature. Cracking rate of Colmonoy 69 deposits was evaluated as the number of cracks per unit area of the coatings. Deposition of the other two clad materials was performed on substrates at room temperature. Dilution from the substrate calculated by dividing the area of the remelted substrate to the total area of the deposited layer plus remelted substrate (Toyserkani et al., 2005) evaluated from the transversal cross-section Optical Microscopy (OM) images was kept in the range of 5-15 percent by adjusting the laser power.

Samples were cut from the transversal and longitudinal cross sections of the clad layers and prepared by standard mechanical grinding with suspensions containing 9 and 3 μm diamond particles and polishing with colloidal Al_2O_3. Microstructure of the deposits and the crack growth paths were observed by OM. In addition, the microstructural details were analyzed by Scanning Electron Microscopy (SEM) using a Philips XL30

Field Emission Gun SEM. Energy Dispersive Spectroscopy (EDS) was employed to study the elemental distributions in the deposits. EDS maps were taken at accelerating voltages of 5 kV for boron and 20 kV for other elements. Microhardness of the deposits was evaluated by a CSM Revetest machine using Vickers indenter at a load of 4.9 N.

Table 1: Nominal chemical composition of the substrate and coating materials (wt.%).

Material	Ni	Cr	B	Si	C	Fe	Mn	Mo	Cu	W
S355 (substrate)	0.7	0.2	-	0.5	0.1	Bal.	1.6	-	0.3	-
Colmonoy 69	Bal.	14	3	4.5	0.7	4	-	2	2	-
Colmonoy 33	Bal.	6	1	4.3	0.2	1.8	-	-	-	-
Nucalloy 488V	Bal,	20.5	1	6	0.3	7.5	-	-	-	2

3. Results

3.1. Microstructures

Our previous work showed that the microstructure of laser deposited Colmonoy 69 coatings consists of three general components: Cr-rich precipitates such as CrB, Cr_5B_3 and Cr_7C_3, Ni solid solution dendrites and Ni-B-Si binary and ternary eutectic phases including Ni_3B, Ni_2B and Ni_3Si (Hemmati et al., 2013). Also, it was observed that Colmonoy 69 laser deposited coatings develop multiple microstructures from the same composition at different cooling rates (Hemmati et al., 2011). Fig. 1 shows various microstructures of Colmonoy 69 deposits observed by OM. Microstructures 1 to 3 developed in the samples with the same dilutions and hence similar compositions. Types of the constituent phases are designated based on the prior phase identification study (Hemmati et al., 2013). Microstructures 1 to 3 all contain numerous Cr boride and carbide precipitates and a considerable amount of interdendritic eutectic structure. The cooling rate at which these microstructures form gradually decreases from microstructure 1 to microstructure 3. The fourth microstructure forms when the Fe content of the deposits becomes very high (40 wt.% or more) because of substantial dilution from the steel substrate (35 % or higher). In such a condition, excessively high Fe contents modify the solidification path of the alloy (Hemmati et al., 2012), suppress the primary boride and carbide phases and diminish the interdendritic eutectics as it can be seen in microstructure 4 of Fig. 1.

Fig. 2 presents the microstructure of Colmonoy 33 and Nucalloy 488V deposits as observed by OM. It seems that Cr boride and carbide precipitates are disappeared and the content of the interdendritic eutectics is dramatically reduced. Contrary to Colmonoy 69 coatings, the microstructure of Colmonoy 33 and Nucalloy 488V samples deposited at different cladding speeds were all similar. This shows these two alloys are not as sensitive to variations in cooling rate. In addition, no substantial differences could be observed in the size of the dendrite arms in the microstructure of Colmonoy 33 and Nucalloy 488V samples deposited at different cladding speeds.

Although OM could provide a general overview of the microstructures, details of the constituent phases could only be revealed by SEM. Fig. 3 shows SEM Backscatter Electron (BSE) microstructural images of Colmonoy 33 and Nucalloy 488V deposits. Detailed microstructural analyses of Colmonoy 69 samples using SEM as well as Transmission Electron Microscopy (TEM) were done previously and reported elsewhere (Hemmati et al., 2013). Fig. 3 (b) shows that the interdendritic areas in Colmonoy 33 deposits contain at least

three components: the cellular structure, the layered eutectic and the dark spots. Fig. 3(c) reveals that there are rod-shape phases in the microstructure of Nucalloy 488V samples which were not visible in the OM image. Also, the rod-shape phases are surrounded or connected by another phase (Fig. 3(d)) which appeared as the brown interdendritic structure in the OM image of Fig. 2(b).

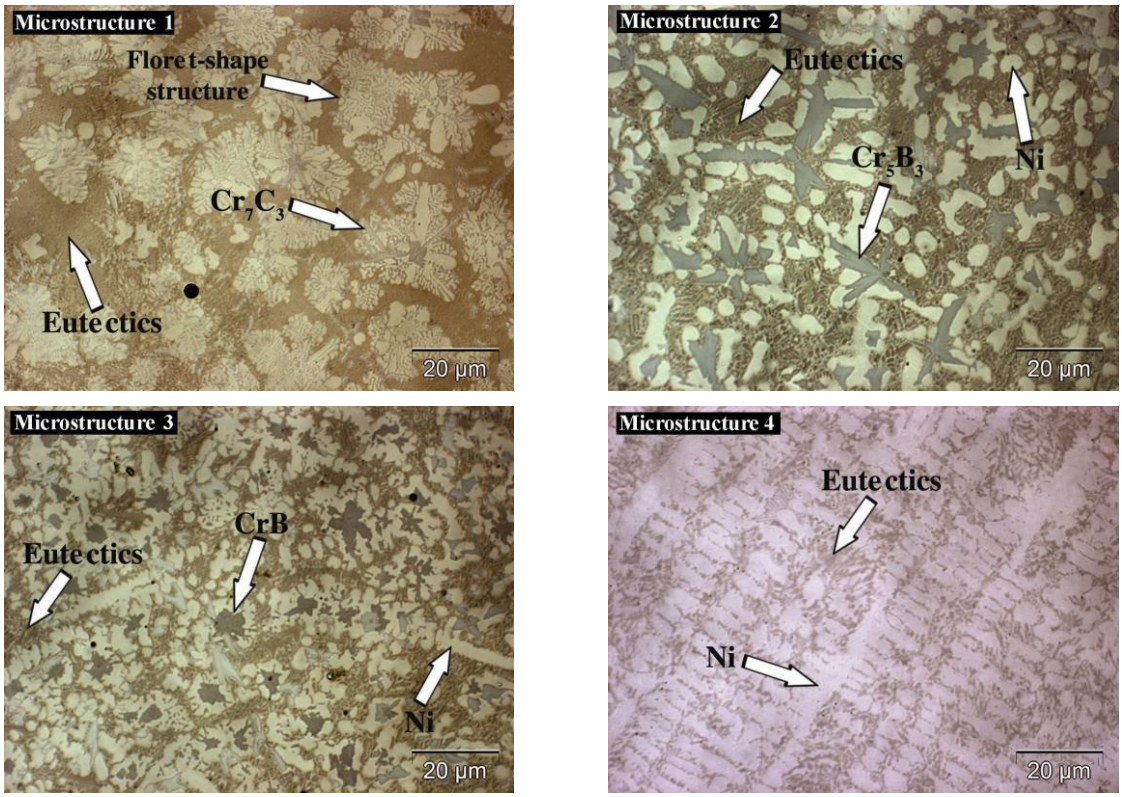

Fig. 1. Various microstructures of Colmonoy 69 deposits observed by OM.

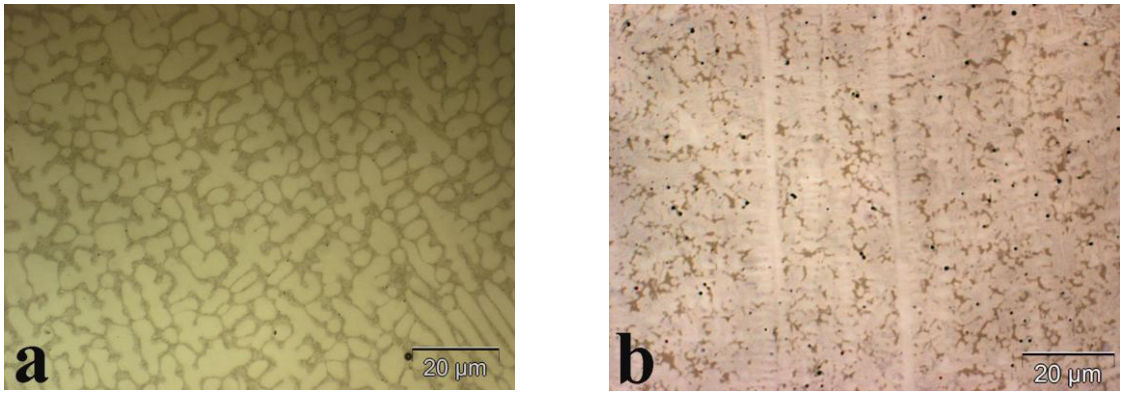

Fig. 2. Microstructure of (a) Colmonoy 33 and (b) Nucalloy 488V observed by OM.

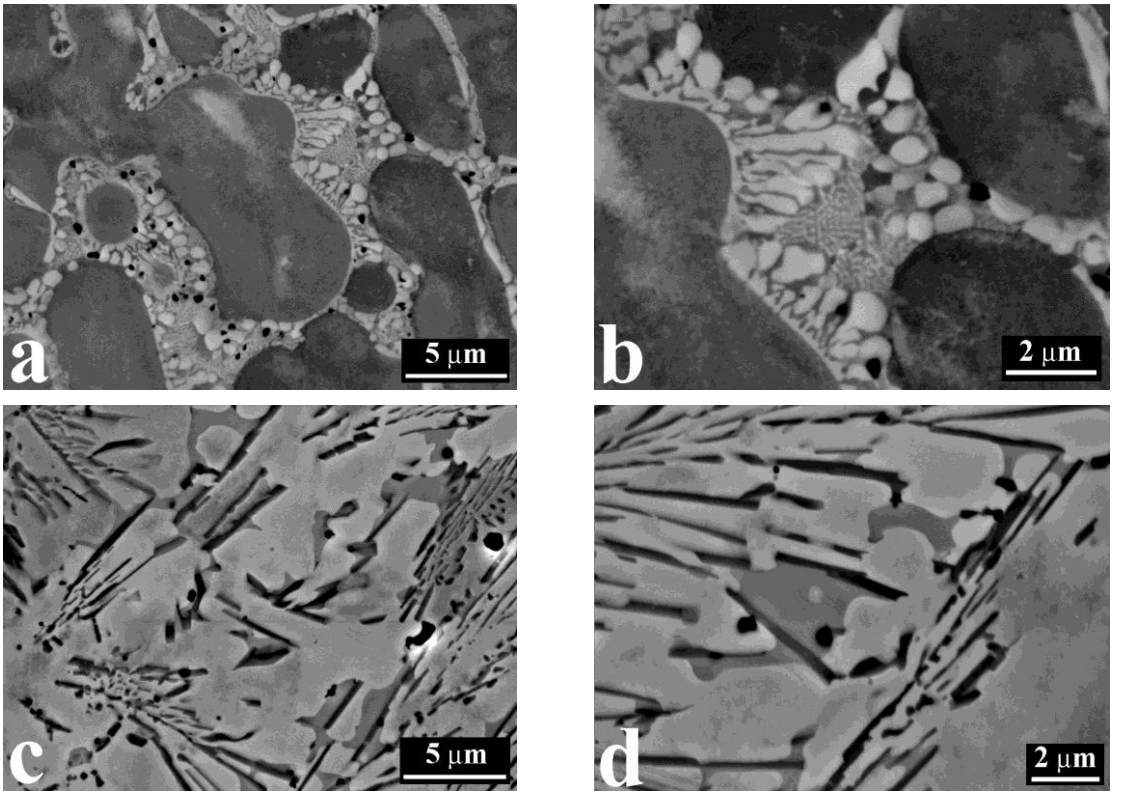

Fig. 3. SEM-BSE images showing the microstructural details of Colmonoy 33 (a and b) and Nucalloy 488V (c and d) at different magnifications.

3.2. Elemental distribution

EDS maps were obtained from several areas of Colmonoy 33 and Nucalloy 488V deposits to assess the distribution of different elements and to get an idea about possible type of the constituent phases visible in Fig. 3. The EDS maps for microstructures of Fig. 3(a) and 3(d) are presented in Fig. 4 and 5 respectively. In Colmonoy 33, both dendrites and interdendritic phases were rich in Ni but segregation of Si and Cr in the interdendritic regions could be found. Based on the EDS maps of Fig. 4, it can be concluded that the interdendritic region of Colmonoy 33 deposits contain Ni-Si eutectics and Cr-rich precipitates (most probably Cr borides). The resolution of EDS mapping was not high enough to conclusively determine the composition of the cellular layers and B or C in the dark Cr-rich precipitates. In the case of Nucalloy 488V deposits, the rod-shape phases were rich in Cr and B and the phases covering and connecting them mostly consisted of Ni and Si. The results of EDS mappings show that the microstructure of both Colmonoy 33 and Nucalloy 488V deposits consist of Ni solid solution dendrites, Ni-Si eutectics and Cr boride precipitates. The amount of Cr borides is much higher in Nucalloy 488V deposits as a result of their higher Cr content.

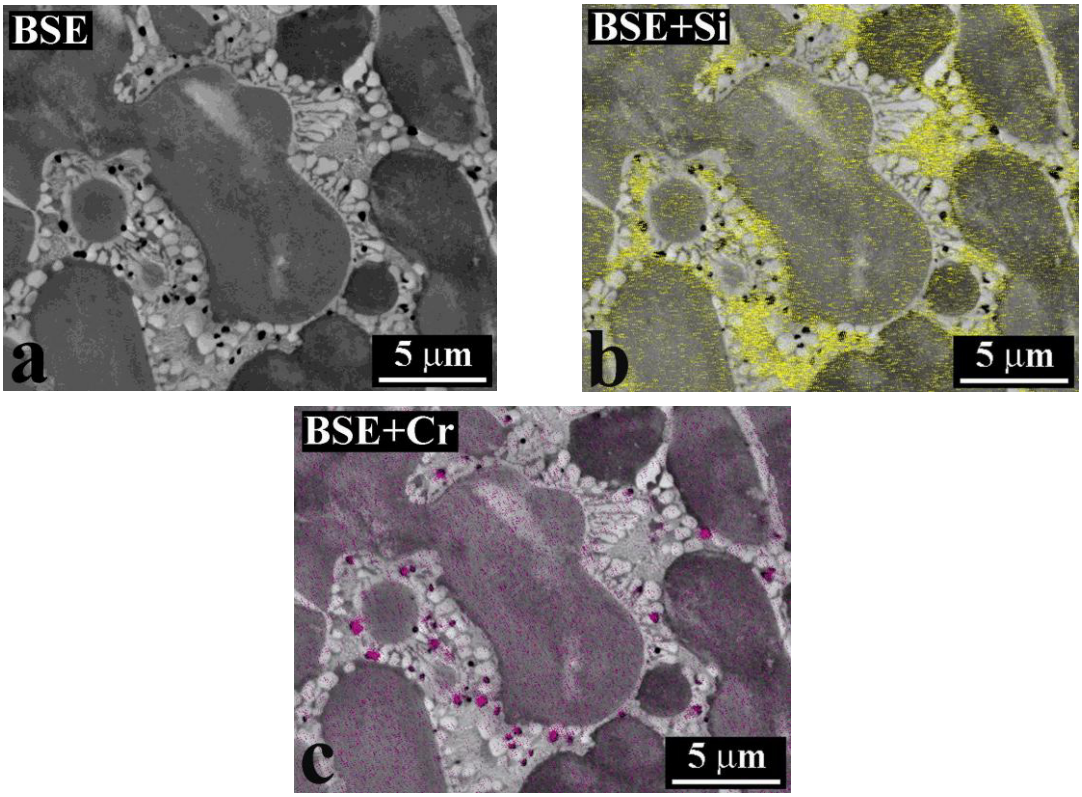

Fig. 4. (a) BSE-SEM microstructural image along with EDS maps in (b) and (c) showing the distribution of Si and Cr in the interdendritic region of Colmonoy 33 deposits. Ni was homogeneously distributed between dendrites and interdendritic regions.

3.3. Hardness and cracking tendency

Hardness values for the different microstructures of Colmonoy 69 as well as Colmonoy 33 and Nucalloy 488V deposits are presented in Fig. 6. Considerable hardness differences existed between various microstructures of Colmonoy 69 shown in Fig. 1. It can be noticed that the hardness of highly-diluted Colmonoy 69 is in the hardness range of Colmonoy 33 and Nucalloy 488V deposits which can be explained by their similar microstructures.

While it was possible to get crack-free Colmonoy 33 and Nucalloy 488V deposits on cold substrates and at all cladding speeds, Colmonoy 69 samples deposited on cold substrates massively cracked and even preheating the substrate to 500 ^{o}C could produce crack-free Colmonoy 69 coatings only at the lowest cladding speed as shown in Fig. 7(a). Studying the crack growth path revealed that both Cr-rich precipitates and the continuous eutectic network contributed to crack propagation process. On the other hand, the Ni solid solution dendrites effectively deflected the growing crack as visible in Fig 7(b).

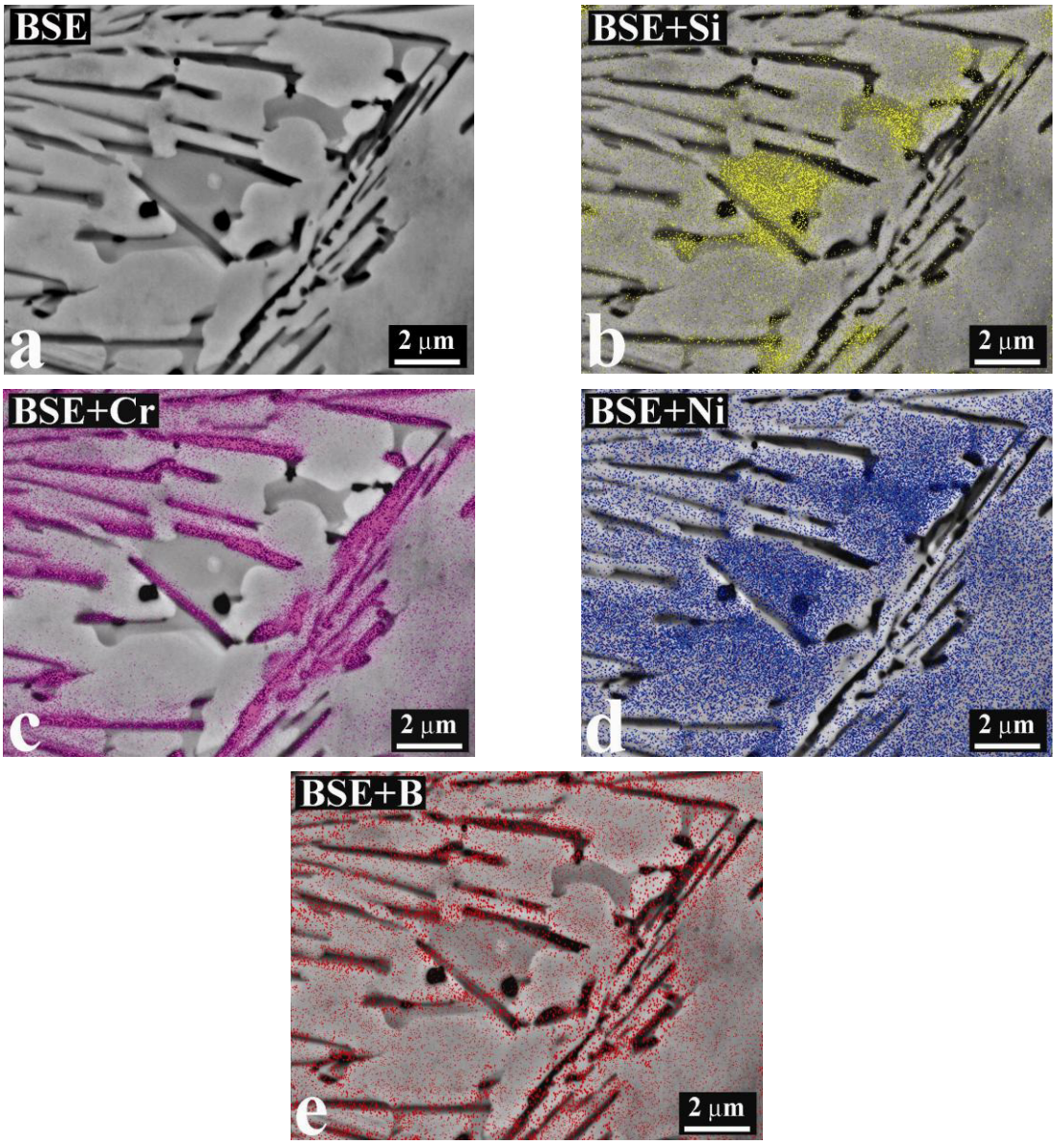

Fig. 5. BSE-SEM image in (a) combined with EDS maps for Si, Cr, Ni and B in (b) to (e) showing the elemental distribution in the microstructure of Nucalloy 488V deposits.

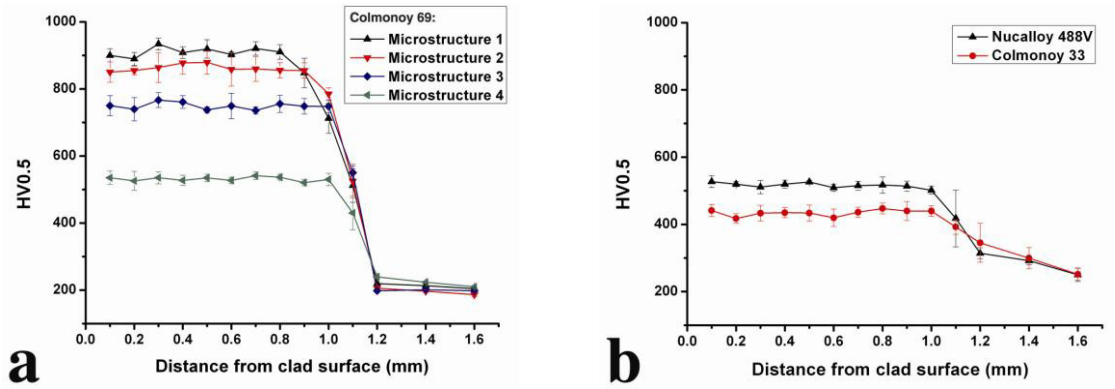

Fig. 6. Hardness graphs for (a) various microstructures of Colmonoy 69 as shown in Fig. 1 and (b) Colmonoy 33 and Nucalloy 488V.

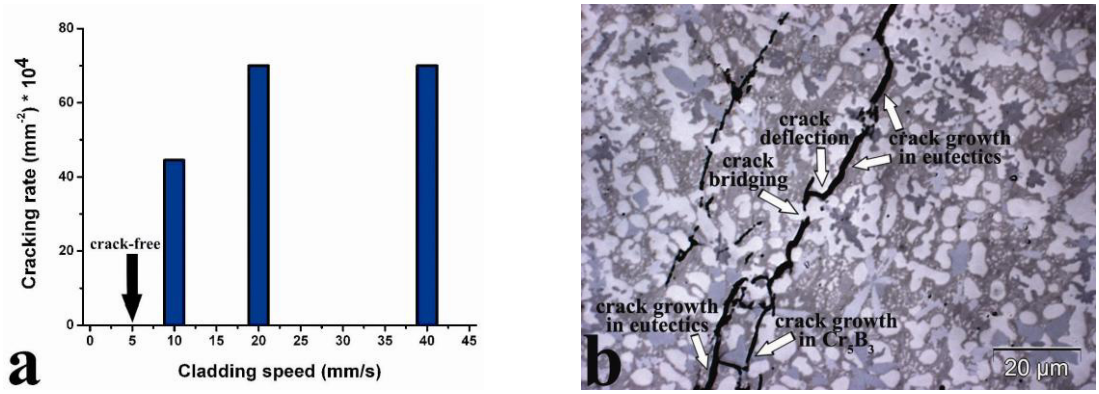

Fig. 7. (a) Cracking rate for Colmonoy 69 clad layers deposited at different speeds on steel substrates preheated to 500 °C, (b) OM image showing a typical crack propagation path in Colmonoy 69 deposits. Propagation of cracks through Cr borides or eutectic network and its deflection by Ni dendrtites are highlighted.

4. Discussions

Based on the above-mentioned results, it is possible to group the Ni-Cr-B-Si alloys into two general categories: the high-alloy grades such as Colmonoy 69 and the low-alloy or dilute grades like Colmonoy 33. Microstructure of laser deposited samples from the first category contains considerable quantities of Cr-rich precipitates (mainly borides) and substantial amounts of interdendritic eutectic structures. In high-alloy grades, abundance of hard Cr-rich precipitates and eutectic structures produces high hardness levels but at the same time provides easy routes for crack propagation as shown in Fig 7(b). Depleting the high-alloy grades out of Cr and B will result in dilute alloys such as Colmonoy 33 in which Cr-rich precipitates are almost eliminated and the eutectic network is substantially diminished. Both of these microstructural changes help to

improve the toughness of the laser deposited coatings but not without losing the high hardness of high-alloy grades. Previous research confirmed that Ni-Cr-B-Si hardfacing alloys (especially the high-alloy grades) have lower fracture toughness values in comparison to their Co- or Fe-base counterparts (Cockeram, 2002). The low fracture toughness of Ni-Cr-B-Si alloys means that crack-free Ni-Cr-B-Si laser deposited coatings and 3-dimentional structures will be difficult to obtain (especially from the high-alloy grades) unless the high cooling rates associated with laser deposition processes are lowered by relatively high substrate preheating temperatures, e.g. 500 ^{o}C or even higher for deposition of Colmonoy 69.

Both quantity and nature of the Ni-B-Si eutectic phases have a substantial effect on hardness and toughness of laser deposited Ni-Cr-B-Si coatings (Hemmati et al., 2011; Kanichi & Hidaka, 1984). Nature of the eutectic structure in Ni-Cr-B-Si deposits is controlled by the Si/B ratio (Kanichi & Hidaka, 1984). For Si/B ratios of less than 3, the eutectic structure will mostly consist of Ni-Ni_3B eutectic which is very hard and brittle. When this ratio is increased to above 3, the primary eutectic reaction will change to Ni-Si type and Ni-Ni_3Si will be the dominant eutectic structure which is softer and less brittle in comparison to the former case. The EDS maps of Fig. 4 and Fig. 5 confirmed that the interdendritic structures in Colmonoy 33 and Nucalloy 488V are rich in Si (and Ni) as expected from their high values of Si/B ratio (around 4 and 6 for Colmonoy 33 and Nucalloy 488V respectively). On the other hand, earlier TEM phase identification studies confirmed that the dominant eutectic structure in Colmonoy 69 deposits (with a Si/B ratio of around 1.5) is Ni-Ni_3B (Hemmati et al., 2013).

Phase formation reactions in Ni-Cr-B-Si alloy system primarily depend on the quantities of Cr, Si, B and consequently the Si/B ratio. If an increase of Si/B ratio is accompanied by a reduction in the Cr content as in Colmonoy 33, not only the nature of the eutectic phases changes from Ni-Ni_3B to Ni-Ni_3Si, but also the Cr borides will be significantly diminished from the microstructure of laser deposited samples. According to the Ni-B and Ni-Si phase diagrams (Baker, 1992), B has a negligible solubility in Ni while Ni may dissolve up to 8.2 wt.% of Si. As a result, relatively high ratios of Si/B are needed to change the nature of the eutectic phases which form at the latest stages of solidification. Insolubility of B in Ni also means that even at higher Si/B ratios (usually equivalent to low B contents), borides can still form if enough Cr is available. This is the case for Nucalloy 488V in which a high ratio of Si/B is combined with a very high Cr content. The outcome is modification of the eutectic structures while keeping some of the Cr borides in the microstructure and hence obtaining a suitable combination of hardness and toughness in the laser deposited samples.

An interesting characteristic of high-alloy Ni-Cr-B-Si grades is their microstructural sensitivity to variations of cooling rates during solidifications as shown in Fig. 1. This characteristic is mostly because of the more complex phase constitution of high-alloy Ni-Cr-B-Si grades and their possibility to follow various solidification paths in comparison to low-alloy grades. As the thermal conditions are usually not constant during laser deposition processes, such sensitivity may cause heterogeneities in microstructure and properties of laser deposited high-alloy Ni-Cr-B-Si grades. Consequently, in addition to high cracking tendency and the necessity of substantial preheating and postheating, microstructural instability can be another issue in laser deposition of the high-alloy members of the Ni-Cr-B-Si family.

5. Conclusions

Three Ni-Cr-B-Si hardfacing alloy powders with different ratios of Si to B and Cr content were deposited at 5-40 mm/s on steel substrate using laser beam and the microstructure, elemental distribution, hardness and cracking tendency of the deposits were studied. The microstructure of Colmonoy 69 deposits with high Cr

content and a low Si to B ratio (Si/B = 1.5) contained numerous Cr boride precipitates and substantial quantities of interdendritic Ni-B-Si eutectics. The abundance of hard Cr-rich precipitates and the eutectic structures produced high hardness levels in Colmonoy 69 deposits but also provided easy routes for crack propagation. The lower Cr content and higher Si/B ratio in Colmonoy 33 eliminated the borides and modified the nature of the eutectic phases in Colmonoy 33 deposits. The microstructure of Nucalloy 488V coatings was a compromise between those of Colmonoy 69 and Colmonoy 33 in which the eutectic structure was of Ni-Si type similar to Colmonoy 33 but much more Cr borides were formed in comparison to Colmonoy 33 as a result of the higher Cr content in Nucalloy 488V. While crack-free Colmonoy 33 or Nucalloy 488V coatings with a hardness of 400-500 HV could be deposited on cold substrates, crack-free coatings from Colmonoy 69 could only be obtained at the lowest cladding speed and after preheating the substrate to 500 ^{o}C.

Acknowledgements

This research was carried out under project number MC7.06259 in the framework of the Research Program of the Materials innovation institute M2i (www.m2i.nl). The Wall Colmonoy Ltd. (The UK) is acknowledged for providing Colmonoy 69 and Colmonoy 33 powders.

References

ANGELASTRO, A., CAMPANELLI, S. L. & LUDOVICO, A. D. (2009). Characterization of Colmonoy 227-F Samples Obtained by Direct Laser Metal Deposition. *Advanced Materials Research* **83-86**, 842–849.

BAKER, H. (ed.) (1992). *ASM Handbook-Alloy Phase Diagrams*. 10th ed. Ohio: ASM International.

COCKERAM, B. V. (2002). The fracture toughness and toughening mechanisms of nickel-base wear materials. *Metallurgical and Materials Transactions A* **33**, 33–56.

CONDE, A., ZUBIRI, F. & DE DAMBORENEA, Y J. (2002). Cladding of Ni–Cr–B–Si coatings with a high power diode laser. *Materials Science and Engineering: A* **334**, 233–238.

DAS, C. R., ALBERT, S. K., BHADURI, A. K., SUDHA, C. & TERRANCE, A. L. E. (2005). Characterisation of nickel based hardfacing deposits on austenitic stainless steel. *Surface Engineering* **21**, 290–296.

FERNÁNDEZ, E., CADENAS, M., GONZÁLEZ, R., NAVAS, C., FERNÁNDEZ, R. & DAMBORENEA, J. DE (2005). Wear behaviour of laser clad NiCrBSi coating. *Wear* **259**, 870–875.

HEMMATI, I., OCELIK, V. & DE HOSSON, J. T. M. (2011). Evolution of microstructure and properties in laser cladding of a Ni-Cr-B-Si hardfacing alloy. In *Contact Mechanics and Surface Treatments X*, pp. 287–296. Malta: WIT Press.

HEMMATI, I., OCELÍK, V. & DE HOSSON, J. T. M. (2012). Dilution effects in laser cladding of Ni–Cr–B–Si–C hardfacing alloys. *Materials Letters* **84**, 69–72.

HEMMATI, I., RAO, J. C., OCELÍK, V. & DE HOSSON, J. T. M. (2013). Electron Microscopy Characterization of Ni-Cr-B-Si-C Laser Deposited Coatings. *Microscopy and Microanalysis* 1–12.

KANICHI, T. & HIDAKA, K. (1984). Hard Facing Nickel-Base Alloy.

MIGUEL, J. M., GUILEMANY, J. M. & VIZCAINO, S. (2003). Tribological study of NiCrBSi coating obtained by different processes. *Tribology International* **36**, 181–187.

PAUL, C. P., JAIN, A., GANESH, P., NEGI, J. & NATH, A. K. (2006). Laser rapid manufacturing of Colmonoy-6 components. *Optics and Lasers in Engineering* **44**, 1096–1109.

PLANCHE, M. P., LIAO, H., NORMAND, B. & CODDET, C. (2005). Relationships between NiCrBSi particle characteristics and corresponding coating properties using different thermal spraying processes. *Surface and Coatings Technology* **200**, 2465–2473.

TOYSERKANI, E., KHAJEPOUR, A. & CORBIN, S. (2005). *Laser cladding*. CRC Press.